J. Korean Soc. Ind. Appl. Math. Vol.27, No.4, 207–231, 2023 https://doi.org/10.12941/jksiam.2023.27.207

AN IMPROVED ALTERNATIVE WENO SCHEMES WITH PERTURBATIONAL TERMS FOR THE HYPERBOLIC CONSERVATION LAWS

KUNMIN SUNG[1], YOUNGSOO HA[1], AND MYUNGJOO KANG[1,†]

[1] DEPARTMENT OF MATHEMATICAL SCIENCES AND RESEARCH INSTITUTE OF MATHEMATICS, SEOUL NATIONAL UNIVERSITY, SEOUL 08826, SOUTH KOREA

Email address: †mkang@snu.ac.kr

ABSTRACT. This paper aims to improve the alternative formulation of the fifth- and sixth-order accurate weighted essentially non-oscillatory (AWENO) finite difference schemes. The first is to derive the AWENO scheme with sixth-order accuracy in the smooth region of the solution. Second, a new weighted polynomial functions combining the perturbed forms with conserved variable to the AWENO is constructed; the new form of tunable functions are invented to maintain non-oscillatory property. Detailed numerical experiments are presented to illustrate the behavior of the new perturbational AWENO schemes. The performance of the present scheme is evaluated in terms of accuracy and resolution of discontinuities using a variety of one and two-dimensional test cases. We show that the resulted perturbational AWENO schemes can achieve fifth- and sixth-order accuracy in smooth regions while reducing numerical dissipation significantly near singularities.

1. INTRODUCTION

The hyperbolic conservation law appears frequently in scientific or engineering applications. It has the nature of allowing discontinuities that cause difficulties to obtain high accuracy numerical solutions. The TVD schemes [1, 2] are very efficient for suppressing the spurious oscillations in numerical solution, however it degenerates accuracy near extrema. The ENO scheme [3, 4, 5, 6, 7] yields non-oscillatory solution by selecting smoothest stencil. The first WENO method introduced by Liu, Osher and Chan [8] had a finite volume form with third-order accuracy in smooth regions. WENO family schemes achieve the non-oscillatory property from non-linear combination of all candidate stencils. A finite difference form of WENO which is very efficient for multidimensional problems, was devised by Jiang and Shu [9] (hereafter WENO-JS). Although the WENO-JS method loses the optimal order at critical points, it is a general framework for WENO schemes.

The mapped WENO scheme (WENO-M) [10] adopts a mapping function to adjust weights of WENO-JS, so it requires more computational cost compared to WENO-JS. The WENO-Z [11] was proposed to derive maximal rate of convergence and to obtain improved results

Received October 11 2023; Revised November 16 2023; Accepted in revised form November 17 2023; Published online December 25 2023.

† Corresponding author.

near discontinuities. Acker, Borges, Costa [12] appended a new term to the smoothness indicator and increased the relevance of less-smooth sub-stencils. Another fifth-order WENO schemes modifying nonlinear weights [13, 14, 15, 16] are further proposed to improve solutions. Hu, Wang, and Adams [17, 18] proposed another version of the sixth-order WENO scheme (WENO-CU) using a new smoothness indicator. In addition, accuracy of WENO scheme has been improved continuously [19, 20, 21]. The central WENO schemes [22, 23, 24], hybrid compact WENO schemes [25, 26], and other versions of the WENO methods [27, 28, 29, 30, 31, 32] have been suggested by many researcher to improve the accuracy of the solutions.

Zeng, Shen and Liu [33] introduced perturbational WENO (P-WENO) scheme with the perturbed candidate fluxes in the WENO-Z schemes. They proved that P-WENO has the sufficient conditions for fifth-order convergence even at critical points. Wang et al. [34] improved the P-WENO scheme by modified smoothness indicators adding a perturbed cubic polynomial approximation of the numerical flux on each candidate stencil using the weights of the WENO-JS scheme.

Since the classical finite difference WENO method for solving the hyperbolic conservation law utilizes a very diffusive flux division, their solutions are not accurate as expected. So, Jiang, Shu, and Zhang [35] proposed a fifth-order alternative WENO method using Lax-Wendroff time discretization (referred to as AWENO). The AWENO methods obtain the numerical results by reconstructing conservative variables, whereas the classical WENO methods obtain the results through the reconstruction of the flux function. Also, AWENO can apply any monotone flux function for the numerical flux, whereas the classic WENO finite difference methods use only smooth flux splitting to reconstruct the flux function.

Even though AWENO has complex implementations, it takes an advantage of various numerical fluxes corresponding to high-order accuracy finite volume method. The AWENO method demonstrates high resolution for fine structures and maintains non-oscillatory property near discontinuities, because it has less dissipation and dispersion error when compared to the WENO method [35]. Furthermore, the AWENO scheme automatically preserves the free-stream in the curvilinear meshes [36]. Liu [37] investigated the performance of several numerical fluxes coupled with AWENO scheme(AWENO-JS). Since the AWENO-JS fail to yield the optimal order of accuracy at the critical points, Wang et al. [38] porposed the AWENO-Z scheme which is employed the WENO-Z nonlinear weights [11, 39] to maintain optimal order of accuracy at the critical points. Liu and Qiu [40] applied AWENO approach to Hermite WENO scheme. Wang, Don, Garg, and Kurganov [41] announced characteristicwise alternative WENO-Z finite-difference schemes, which adaptively adjusts the numerical diffusion coefficient for the compressible Euler gas dynamics equations.

In this paper, we develop the perturbational AWENO schemes which are adding the perturbed terms to the candidate conservative variables to construct a new weighted scheme for fifth order AWENO-JS and AWENO-Z and sixth order AWENO-CU. First, we formulate the perturbational AWENO schemes to the fifth order AWENO-JS and AWENO-Z schemes. We propose the sixth order AWENO scheme from modifying the WENO-CU scheme and develop the corresponding coefficients of the perturbed terms to yield the sixth order smooth regions

even at critical points. Comparing with other AWENO schemes, the proposed schemes yield better approximations with perturbational terms. A number of numerical experiments are presented to illustrate the behavior of the new AWENO scheme.

The rest of this paper is organized as follows. Section 2 gives a brief review of the AWENO. In Section 3, a perturbational AWENO scheme is introduced with new tunable functions which controls the contribution of perturbational terms. In Section 4, we address the low dissipation and robustness of the proposed schemes with detailed numerical tests. Some conclusions of this paper are given in Section 5.

2. **AWENO schemes**

We depict a formula of AWENO schemes in this section. The hyperbolic conservation law can be explained reasonably in one-dimensional spacial coordinate x and temporal coordinate t :

$$\begin{aligned} &u_t + f(u)_x = 0, \quad t \geq 0,\ x \in \mathbb{R}, \\ &u(x,0) = u_0(x), \end{aligned} \tag{2.1}$$

under proper boundary conditions. Here, the vector $u = (u_1, \cdots, u_m)$ represents conserved quantities, and $f(u)$ is a vector-valued function with m components. The computational domain is partitioned into uniform cells $I_j = [x_{j-1/2}, x_{j+1/2}]$ and $\Delta x = x_{j+1/2} - x_{j-1/2}$ denote the cell size. The centers of each cell are denoted by the points $\{x_{j+1/2}\}$. In particular, $f_j := f(u(x_j,t))$ represents the function value at the node x_j.

2.1. **Formulation of AWENO scheme.**

At each node x_j, the semi-discretized form of the Eq. (2.1) generates a system of ODE (ordinary differential equation) by the method of lines:

$$\frac{du_j}{dt} = -\frac{\partial f}{\partial x}\Big|_{x=x_j} \tag{2.2}$$

where $u_j(t)$ is an approximate value to the value $u(x_j,t)$ in a grid. The spatial derivative $\frac{\partial f}{\partial x}\Big|_{x=x_j}$ in (2.2) can be approximated by the following conservative scheme

$$\frac{\partial f}{\partial x}\Big|_{x=x_j} = -\frac{\hat{f}_{j+\frac{1}{2}} - \hat{f}_{j-\frac{1}{2}}}{\Delta x}$$

where the numerical flux $\hat{f}_{j+\frac{1}{2}} = \hat{f}(u_{j-r}, \cdots, u_{j+s})$ with $r+s = k-1$ is designed to become a kth-order scheme.

We now briefly describe the alternative WENO (AWENO) schemes in one dimensional scalar cases (2.1). The numerical flux of the AWENO method proposed by Jiang et al. [35] takes a new type of numerical flux that is different from the flux used in the classical WENO method. AWENO's numerical flux $\hat{f}$ is a form of adding a high-order numerical flux $\hat{f}^{HO}$ to the low-order numerical flux $\hat{f}^{LO}$; $\hat{f}_{j+\frac{1}{2}} = \hat{f}^{HO}_{j+\frac{1}{2}} + \hat{f}^{LO}_{j+\frac{1}{2}}$. Any monotone flux can be used

for the low-order numerical flux $\hat{f}^{LO}$. We use the Lax-Friedrichs or HLLC flux function in Appendix. The high-order numerical flux $\hat{f}^{HO}$ is defined by

$$\hat{f}^{HO}_{j+\frac{1}{2}} = \sum_{l=1}^{[(k-1)/2]} a_{2l} \Delta x^{2l} \left(\frac{\partial^{2l}}{\partial x^{2l}} f \right)_{j+\frac{1}{2}} + \mathcal{O}(\Delta x^{k+1}).$$

In order to achieve fifth- and sixth-order accuracy AWENO schemes, we obtain the coefficients a_{2l} from the Taylor series expansion. Thus we have

$$\hat{f}^{HO}_{j+\frac{1}{2}} = -\frac{1}{24}(\Delta x)^2 (f_{xx})_{j+\frac{1}{2}} + \frac{7}{5760}(\Delta x)^4 (f_{xxxx})_{j+\frac{1}{2}} + \mathcal{O}(\Delta x^6).$$

The the second and fourth derivatives are approximated from the standard central finite differences method with an overall global accuracy $\mathcal{O}(\Delta x^6)$, that is

$$\begin{aligned} \Delta x^2 f_{xx}\Big|_{j+\frac{1}{2}} &= \frac{1}{48}(-5f_{j-2} + 39f_{j-1} - 34f_j - 34f_{j+1} + 39f_{j+2} - 5f_{j+3}) + \mathcal{O}(\Delta x^6), \\ \Delta x^4 f_{xxxx}\Big|_{j+\frac{1}{2}} &= \frac{1}{2}(f_{j-2} - 3f_{j-1} + 2f_j + 2f_{j+1} - 3f_{j+2} + f_{j+3}) + \mathcal{O}(\Delta x^6). \end{aligned} \tag{2.3}$$

2.2. **WENO interpolations.** The kth-order accuracy WENO interpolation uses the convex combination of rth-order polynomial approximation $p^{(r)}_{j+\frac{1}{2}}$ obtained based on r-th point substencil

$$u^-_{j+\frac{1}{2}} = \sum_{r=0}^{k-1} \omega_r p^{(r)}_{j+\frac{1}{2}} \tag{2.4}$$

where ω_r are the nonlinear weights. In order to obtain ω_r, we are using optimal (or ideal) weights d_r and applying the improved nonlinear weights which are introduced by Borges at al. [11]:

$$\omega_r = \frac{\alpha_r}{\sum_{\ell=0}^{k-1} \alpha_\ell}, \qquad \alpha_r = d_r \Big[1 + \Big(\frac{\tau_{2k-1}}{\beta_r + \varepsilon} \Big) \Big], \qquad r = 0, 1, \ldots, k-1$$

where a small positive value $\varepsilon > 0$ is employed to prevent the division by zero and τ_{2k-1} is the global (optimal order) smoothness indicator. The local smoothness indicator β_r introduced by Jiang and Shu [9] is given by

$$\beta_r = \sum_{\ell=1}^{k-1} \int_{x_{j-1/2}}^{x_{j+1/2}} \Delta x^{2\ell-1} \Big(\frac{d^\ell}{dx^\ell} p^{(r)} \Big)^2 dx, \quad r = 0, 1, \ldots, k-1. \tag{2.5}$$

The reconstruction to $u^+_{j+\frac{1}{2}}$ is mirror symmetric to that for $u^-_{j+\frac{1}{2}}$ from $\{x_{j-r+1}, \ldots, x_{j+s+1}\}$.

2.2.1. *The fifth-order WENO interpolation.* The fifth-order WENO interpolation is to combine the three second-order polynomial approximations on the stencils

$$G_5 := \{x_{j-2}, \dots, x_{j+2}\}$$

which is subdivided into three candidate substencils $\mathcal{S}_r := \{x_{j+r-2}, x_{j+r-1}, x_{j+r}\}$, $r = 0, 1, 2$.

We would derive the three parabolic interpolants $p^{(r)}$ from the candidate substencils $\mathcal{S}_r$ for $r = 0, 1, 2$ and then weights ω_r are assigned to each parabolic interpolant $p^{(r)}$ to construct the fifth-order WENO interpolation. Then the three interpolants are given by

$$\begin{aligned} p^{(0)}_{j+\frac{1}{2}} &= \frac{3}{8}u_{j-2} - \frac{5}{4}u_{j-1} + \frac{15}{8}u_j, \\ p^{(1)}_{j+\frac{1}{2}} &= -\frac{1}{8}u_{j-1} + \frac{3}{4}u_j + \frac{3}{8}u_{j+1}, \\ p^{(2)}_{j+\frac{1}{2}} &= \frac{3}{8}u_j + \frac{3}{4}u_{j+1} - \frac{1}{8}u_{j+2}. \end{aligned} \tag{2.6}$$

The final WENO interpolation is defined by a convex combination of these functions with weights ω_r in Eq. (2.4). The specific values of d_r are known as $d_0 = \frac{1}{16}$, $d_1 = \frac{10}{16}$ and $d_2 = \frac{5}{16}$. The $\tau_5 = |\beta_0 - \beta_2|$ is used for the global (optimal order) smoothness indicator. The smoothness indicators are given by

$$\begin{aligned} \beta_0 &= \frac{1}{4}(u_{j-2} - 4u_{j-1} + 3u_j)^2 + \frac{13}{12}(u_{j-2} - 2u_{j-1} + u_j)^2, \\ \beta_1 &= \frac{1}{4}(u_{j-1} - u_{j+1})^2 + \frac{13}{12}(u_{j-1} - 2u_j + u_{j+1})^2, \\ \beta_2 &= \frac{1}{4}(3u_j - 4u_{j+1} + u_{i+2})^2 + \frac{13}{12}(u_j - 2u_{j+1} + u_{j+2})^2. \end{aligned} \tag{2.7}$$

2.2.2. *The sixth-order WENO interpolation.* For the sixth-order WENO interpolation, we use a six point stencil

$$G_6 := \{x_{j-2}, \dots, x_{j+3}\}$$

having the four second order polynomials $p^{(r)}$ on the four substencils $\mathcal{S}_r := \{x_{j+r-2}, \dots, x_{j+r}\}$, $r = 0, 1, 2, 3$. The nonlinear weights ω_r and optimal weights d_r can be obtained by a similar way for the fifth-order WENO methods. Then the global solution $u^-_{j+\frac{1}{2}}$ is obtained by a convex combination of the local solutions $p^{(r)}_{j+\frac{1}{2}}$ with $r = 0, 1, 2, 3$:

$$u^-_{j+\frac{1}{2}} = \sum_{r=0}^{3} \omega_r p^{(r)}_{j+\frac{1}{2}}$$

where $\{\omega_r : r = 0, \cdots, 3\}$ are nonlinear weights. The $p^{(r)}, r = 0, 1, 2$, are the same with those of fifth-order WENO schemes and the last $p^{(3)}$ is assigned by

$$p^{(3)}_{j+\frac{1}{2}} = \frac{15}{8}u_{j+1} - \frac{5}{4}u_{j+2} + \frac{3}{8}u_{j+3}.$$

In order to retain the sixth-order convergence, the specific values of d_k are computed as $d_0 = \frac{1}{32}$, $d_1 = d_2 = \frac{15}{32}$ and $d_3 = \frac{1}{32}$. Further, using these numbers d_r, the nonlinear weights ω_r are defined by

$$\omega_r = \frac{\alpha_r}{\sum_{\ell=0}^{3} \alpha_\ell}, \quad \alpha_r = d_r\Big(1 + \frac{\tau_6}{\varepsilon + \beta_r}\Big), \quad r = 0, 1, 2, 3, \tag{2.8}$$

where $\tau_6 = \beta_6 - \frac{1}{6}(\beta_0 + 4\beta_1 + \beta_2)$ and $\varepsilon = 10^{-20}$ are employed to prevent the denominator becoming zero. For the sixth-order WENO interpolation, the smoothness indicator β_3 is replaced by β_6 which is obtained by calculating (2.5) with the sixth-order interpolation, that is

$$\begin{aligned}\beta_3 = \beta_6 = \frac{1}{12 \cdot 10080}\big[&271779u_{j-2}^2 + u_{j-2}(-2380800u_{j-1} + 4086352u_j - 3462252u_{j+1} + 1458762u_{j+2} - 245620u_{j+3}) \\ &+ u_{j-1}(5653317u_{j-1} - 20427884u_j + 17905032u_{j+1} - 7727988u_{j+2} + 1325006u_{j+3}) + u_j(19510972u_j \\ &- 35817664u_{j+1} + 15929912u_{j+2} - 2792660u_{j+3}) + u_{j+1}(17195652u_{j+1} - 15880404u_{j+2} + 2863984u_{j+3}) \\ &+ u_{j+2}(3824847u_{j+2} - 1429976u_{j+3}) + 139633u_{j+3}^2\big].\end{aligned}$$

3. THE PERTURBATIONAL WENO INTERPOLATIONS

In this section, we will introduce modified WENO interpolations by adding high-order correctional terms to each parabolic interpolant $p^{(r)}$ in Eq. (2.6) to improve solutions nearby discontinuities.

3.1. **The fifth-order case.**

Firstly, we will modify the parabolic interpolants (2.6) with Taylor expansions with respect to $u_{j+\frac{1}{2}}$ on the stencils $G_5 := \{x_{j-2}, \ldots, x_{j+2}\}$. Then we get the following formulas

$$\begin{aligned} p_{j+\frac{1}{2}}^{(0)} &= u_{j+\frac{1}{2}} - \frac{5}{16}\Delta x^3 u'''_{j+\frac{1}{2}} + \mathcal{O}(\Delta x^4), \\ p_{j+\frac{1}{2}}^{(1)} &= u_{j+\frac{1}{2}} + \frac{1}{16}\Delta x^3 u'''_{j+\frac{1}{2}} + \mathcal{O}(\Delta x^4), \\ p_{j+\frac{1}{2}}^{(2)} &= u_{j+\frac{1}{2}} - \frac{1}{16}\Delta x^3 u'''_{j+\frac{1}{2}} + \mathcal{O}(\Delta x^4). \end{aligned}$$

If we follow perturbational approach [33], $u'''_{j+\frac{1}{2}}$ approximates to

$$u'''_{j+\frac{1}{2}} = \frac{-u_{j-2} + 2u_{j-1} - 2u_{j+1} + u_{j+2}}{2\Delta x^3} + \mathcal{O}(\Delta x).$$

The WENO interpolations are promoted to fourth-order from the third-order accuracy by introducing the perturbational term. The modified WENO interpolations $\tilde{p}^{(r)}$ on each candidate

substencil at $x_{j+\frac{1}{2}}$ is obtained by the following forms:

$$\begin{aligned}
\tilde{p}^{(0)}_{j+\frac{1}{2}} &= u_{j+\frac{1}{2}} + \frac{5}{32}(-u_{j-2} + 2u_{j-1} - 2u_{j+1} + u_{j+2}),\\
\tilde{p}^{(1)}_{j+\frac{1}{2}} &= u_{j+\frac{1}{2}} - \frac{1}{32}(-u_{j-2} + 2u_{j-1} - 2u_{j+1} + u_{j+2}),\\
\tilde{p}^{(2)}_{j+\frac{1}{2}} &= u_{j+\frac{1}{2}} + \frac{1}{32}(-u_{j-2} + 2u_{j-1} - 2u_{j+1} + u_{j+2}).
\end{aligned} \tag{3.1}$$

Thus we have the global solution $u^{-}_{j+\frac{1}{2}}$ is obtained by $\tilde{p}^{(r)}_{j+\frac{1}{2}}$ with $r = 0, 1, 2$:

$$u^{-}_{j+\frac{1}{2}} = \sum_{k=0}^{2} \omega_k \tilde{p}^{(k)}_{j+\frac{1}{2}}.$$

However, the modified interpolations can be lost the ENO property because of $\Delta x^3 u'''_{j+\frac{1}{2}} = (-u_{j-2} + 2u_{j-1} - 2u_{j+1} + u_{j+2})/2$ in all interpolation. In [33], a tunable function φ_5 is applied to limit the influence of the last terms in Eq. (3.1) and recover the ENO property. The final WENO interpolation is

$$u^{-}_{j+\frac{1}{2}} = \sum_{k=0}^{2} \omega_k p^{(k)}_{j+\frac{1}{2}} + \frac{\varphi_5(5\omega_0 - \omega_1 + \omega_2)}{32}(-u_{j-2} + 2u_{j-1} - 2u_{j+1} + u_{j+2}) \tag{3.2}$$

where $\varphi_5 = \left(\dfrac{2\sqrt{\beta_0\beta_2}}{\beta_0 + \beta_2 + \varepsilon}\right)$ is ratio of the geometric mean to the arithmetic mean for β_0 and β_2. The function φ_5 controls the contribution of $u'''_{j+\frac{1}{2}}$; it has small value when the stencil has discontinuities whereas it closes to 1 in smooth regions.

3.2. **The sixth-order case.** Since the sixth-order WENO interpolation combines the four second-order polynomials $p^{(k)}$, it needs extra polynomial $p^{(3)}$ on stencil $\{x_{j+1}, x_{j+2}, x_{j+3}\}$. The fourth polynomial $p^{(3)}$ also is computed by

$$p^{(3)}_{j+\frac{1}{2}} = u_{j+\frac{1}{2}} + \frac{5}{16}\Delta x^3 u'''_{j+\frac{1}{2}} + \mathcal{O}(\Delta x^4).$$

In order to obtain the sixth-order accurate, $u'''_{j+\frac{1}{2}}$ have to be discretize by

$$u'''\Big|_{j+\frac{1}{2}} = \frac{-u_{j-2} - u_{j-1} + 10u_j - 14u_{i+1} + 7u_{j+2} - u_{j+3}}{4\Delta x^3} + \mathcal{O}(\Delta x)$$

on six points stencil : $\{x_{j-2}, \ldots, x_{j+3}\}$. Thus we have

$$\tilde{p}^{(k)}_{j+\frac{1}{2}} = u_{j+\frac{1}{2}} + A_k \frac{-u_{j-2} - u_{j-1} + 10u_j - 14u_{i+1} + 7u_{j+2} - u_{j+3}}{4\Delta x^3},$$

where $A_0 = \frac{5}{16}$, $A_1 = -\frac{1}{16}$, $A_2 = \frac{1}{16}$ and $A_3 = -\frac{5}{16}$. The tunable function φ_6 is required to restore ENO properties near discontinuities. In this paper, we consider two sub-stencils $\{x_{j-2}, \ldots, x_{j+1}\}$ and $\{x_j, \ldots, x_{j+3}\}$ to construct φ_6. Since each sub-stencil consists of four

points, the third derivative property is available. The closed formula can be written as $\varphi_6 = \left(\frac{2\sqrt{\alpha_1\alpha_2}}{\alpha_1+\alpha_2+\varepsilon}\right)$, where

$$\alpha_1 = (a_1 + \frac{1}{10}a_3)^2 + \frac{13}{3}a_2^2 + \frac{781}{20}a_3^2,$$
$$\alpha_2 = (b_1 + \frac{1}{10}b_3)^2 + \frac{13}{3}b_2^2 + \frac{781}{20}b_3^2$$

and

$$a_1 = \frac{11u_{j-2} + 63u_{j-2} + 33u_{j-1} + 19u_j}{60},\ a_2 = \frac{u_{j-1} - 2u_j + u_{j+1}}{2},$$
$$a_3 = \frac{-u_{j-2} + 3u_{j-2} - 3u_{j-1} + u_j}{6}, b_1 = \frac{-109u_j + 177u_{j+1} - 87u_{j+2} + 19u_{j+3}}{60},$$
$$b_2 = \frac{2u_j - 5u_{j+1} + 4u_{j+2} - 3u_{j+3}}{2},\ b_3 = \frac{-u_j + 3u_{j+1} - 3u_{j+2} + u_{j+3}}{6}.$$

The φ_6 is ratio of the geometric mean to the arithmetic mean for α_1 and α_2. Also, $0 \le \varphi_6 \le 1$ limits the contribution of $u'''_{j+\frac{1}{2}}$. Finally, we have the following form;

$$\begin{aligned} u^-_{j+\frac{1}{2}} &= \sum_{k=0}^{3} \omega_k \tilde{p}^{(k)}_{j+\frac{1}{2}}, \\ &= \sum_{k=0}^{3} \omega_k p^{(k)}_{j+\frac{1}{2}} + \frac{\varphi_6(5\omega_0 - \omega_1 + \omega_2 - 5\omega_3)}{64}(-u_{j-2} - u_{j-1} + 10u_j - 14u_{i+1} + 7u_{j+2} - u_{j+3}). \end{aligned} \tag{3.3}$$

We summarize the overall procedure for perturbed AWENO in Algorithm 1.

(1) compute the interpolants $p^{(r)}_{j+\frac{1}{2}}$ from Eq. (2.6)
(2) compute the β_r and ω_r from Eq. (2.7) and Eq. (2.8), respectively
(3) compute the $u^-_{j+\frac{1}{2}}$ from Eq. (3.2) or Eq. (3.3)
(4) compute the $u^+_{j+\frac{1}{2}}$ with mirror symmetric process of (1), (2) and (3)
(5) compute the $\hat{f}^{LO}_{j+\frac{1}{2}}$ from selected flux function (LF or HLLC)
(6) compute the $\hat{f}^{HO}_{j+\frac{1}{2}}$ from Eq. (2.3)
(7) finally, the numerical flux $\hat{f}_{j+\frac{1}{2}} = \hat{f}^{HO}_{j+\frac{1}{2}} + \hat{f}^{LO}_{j+\frac{1}{2}}$

Algorithm 1: The generalized procedure to obtain flux for perturbed AWENO schemes

4. NUMERICAL RESULTS

In this section, we demonstrate the non-oscillatory property and designed accuracy of the proposed perturbational AWENO schemes with several numerical tests of the hyperbolic conservation laws. The AWENO-Z or AWENO-CU are alternative WENOs based on WENO-Z [11, 39] or sixth-order central upwind [17], respectively. Each scheme can be improved by perturbational terms; the suffix '-P' means perturbational scheme. We start with the accuracy test of the 1D and 2D Euler equations.

4.1. **Convergence Order of AWENO.**

We test the accuracy of the proposed AWENO schemes using the one and two-dimensional Euler equations.

Example 4.1. (*Accuracy test*) It is important that proposed schemes satisfy the desired order of accuracy. Let us consider the convergence order with the Euler equation in one- or two-dimensional coordinate:

$$U_t + F(U)_x + G(U)_y = 0.$$

Here

$$\begin{aligned} U &= (\rho, \rho u, \rho v, E)^T, \\ F(U) &= (\rho u, p + \rho u^2, \rho uv, u(E+p))^T, \\ G(U) &= (\rho v, \rho vu, p + \rho v^2, v(E+p))^T \end{aligned}$$

where ρ is the density, u and v (is 0 for one-dimensional case) are speed for x-axis and y-axis direction respectively; The pressure p has a relation with total energy E i.e. equation of state for ideal gas:

$$E = \frac{p}{\gamma - 1} + \frac{\rho(u^2 + v^2)}{2}$$

where $\gamma = 1.4$ is the ratio of specific heats. The initial data is

$$\rho(x, y, t) = 1 + 0.5\sin(4\pi(x + y)) \text{ with } u = 1,\ v = -1/2, \text{ pressure } p = 1$$

and periodic boundary conditions are employed. We use classical (non-TVD) RK4 [7] with $\Delta t = \Delta x^{6/4}$ and perform the test until the final time $t = 4$. The Lax-Friedrichs (LF) flux function is chosen for $\hat{f}^{LO}$. The L^1- and L^∞- errors of density ρ are presented in Table 1 and 2; all schemes show the desired order of accuracy on refined mesh. The perturbational terms improve AWENO schemes. We notice that the perturbational terms can reduce the excessive dissipation in AWENO schemes while satisfy desirable accuracy; new tunable functions φ_5 and φ_6 properly work on AWENO scheme. The AWENO-CU-P scheme shows good efficiency compared to the other AWENO schemes.

4.2. **1D Euler Systems.**

Let us consider the 1D Euler gas dynamics for ideal gases. The characteristic decomposition [42] is performed to generalize the AWENO methods. The low-order numerical flux $\hat{f}^{LO}$ is the Lax-Fridrich (denoted as LF) or HLLC.

TABLE 1. Order of accuracy on refined grids: L^1 and L^∞ errors of density in the Euler 1D system with smooth periodic initial condition.

	AWENO-Z	AWENO-Z-P	AWENO-CU	AWENO-CU-P
N	L^1-error (order)			
20	1.66E-04 (—)	1.53E-04 (—)	3.51E-05 (—)	3.42E-05 (—)
40	4.72E-06 (5.14)	4.67E-06 (5.03)	4.98E-07 (6.14)	4.95E-07 (6.11)
80	1.45E-07 (5.02)	1.45E-07 (5.01)	7.59E-09 (6.04)	7.58E-09 (6.03)
160	4.51E-09 (5.00)	4.51E-09 (5.01)	1.18E-10 (6.01)	1.18E-10 (6.01)
320	1.41E-10 (5.00)	1.41E-10 (5.00)	2.36E-12 (5.64)	2.36E-12 (5.64)
N	L^∞-error (order)			
20	2.76E-04 (—)	2.40E-04 (—)	5.64E-05 (—)	5.44E-05 (—)
40	7.85E-06 (5.13)	7.46E-06 (5.01)	7.69E-07 (6.20)	7.65E-07 (6.15)
80	2.32E-07 (5.08)	2.32E-07 (5.00)	1.17E-08 (6.04)	1.17E-08 (6.03)
160	7.13E-09 (5.03)	7.13E-09 (5.03)	1.84E-10 (5.99)	1.84E-10 (5.99)
320	2.55E-10 (4.81)	2.55E-10 (4.81)	3.73E-12 (5.63)	3.73E-12 (5.63)

TABLE 2. Orders of accuracy on refined grids: L^1 and L^∞ errors of density in the Euler 2D system with smooth periodic initial condition.

	AWENO-Z	AWENO-Z-P	AWENO-CU	AWENO-CU-P
$N \times N$	L^1-error (order)			
20×20	2.74E-02 (—)	2.03E-02 (—)	6.70E-03 (—)	4.60E-03 (—)
40×40	8.74E-04 (4.97)	7.97E-04 (4.67)	6.32E-05 (6.73)	6.22E-05 (6.21)
80×80	2.62E-05 (5.06)	2.61E-05 (4.93)	8.78E-07 (6.17)	8.74E-07 (6.15)
160×160	8.29E-07 (4.98)	8.29E-07 (4.98)	1.33E-08 (6.04)	1.33E-08 (6.03)
320×320	2.61E-08 (4.99)	2.61E-08 (4.99)	2.20E-10 (5.92)	2.20E-10 (5.92)
$N \times N$	L^∞-error (order)			
20×20	4.63E-02 (—)	3.43E-02 (—)	1.14E-02 (—)	1.00E-02 (—)
40×40	1.40E-03 (5.05)	1.20E-03 (4.84)	1.28E-04 (6.48)	1.14E-04 (6.45)
80×80	4.34E-05 (5.01)	4.10E-05 (4.87)	1.34E-06 (6.57)	1.33E-06 (6.43)
160×160	1.33E-06 (5.03)	1.31E-06 (4.97)	2.14E-08 (5.97)	2.13E-08 (5.96)
320×320	4.14E-08 (5.01)	4.12E-08 (4.99)	3.49E-10 (5.93)	3.49E-10 (5.93)

Example 4.2. (Shock-entropy wave interaction) We apply the proposed AWENO schemes to the shock-entropy wave interaction problem [7]. Since the solution includes an interaction between shock waves and smooth flow features, it is a good model problem to illustrate the superiority of the high-order accuracy. We solve this problem on the interval $[-5, 5]$ with the following initial condition

$$(\rho, u, p) = \begin{cases} (3.857143, 2.629369, 10.33333) & \text{for } x \in [-5, -4), \\ (1 + \varepsilon \sin(kx), 0, 1) & \text{for } x \in [-4, 5]. \end{cases}$$

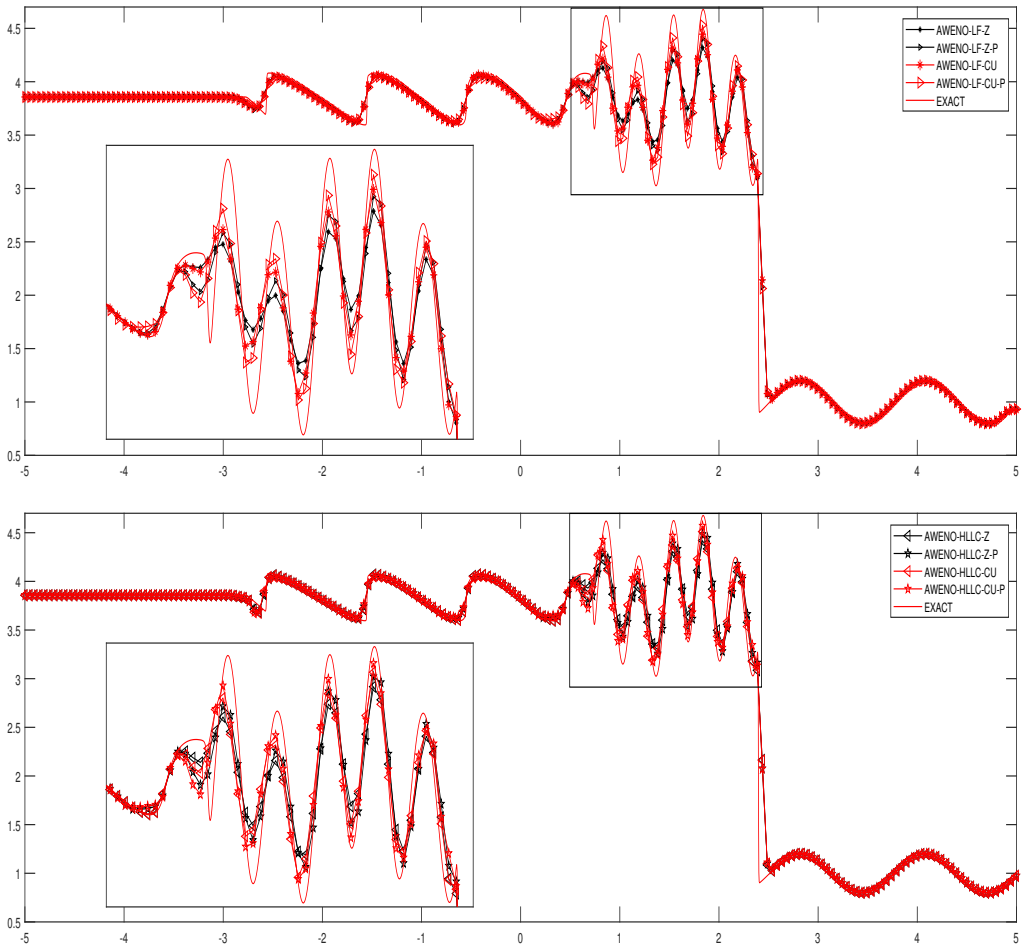

FIGURE 1. Density profiles of the shock-entropy interaction problem [7] with 200 grid points at $t = 1.8$.

Here, $\varepsilon = 0.2$ is the amplitude of the entropy wave and $k = 5$ is wave number of the entropy wave. The shock wave moving with Mach 3 induces wave trails of higher frequency than the original wave number k. We solve this problem with CFL=0.5. We get the referenced "exact" solution by fifth order WENO-JS scheme [9] with 3200 mesh points. The density ρ profiles at $t = 1.8$ are shown in Fig. 1; the non-oscillatory properties can be confirmed. In the magnified view, all AWENO schemes are improved with perturbational terms; the results of LF are significantly improved. The AWENO-CU-P (LF or HLLC) shows good result even in the very corse mesh.

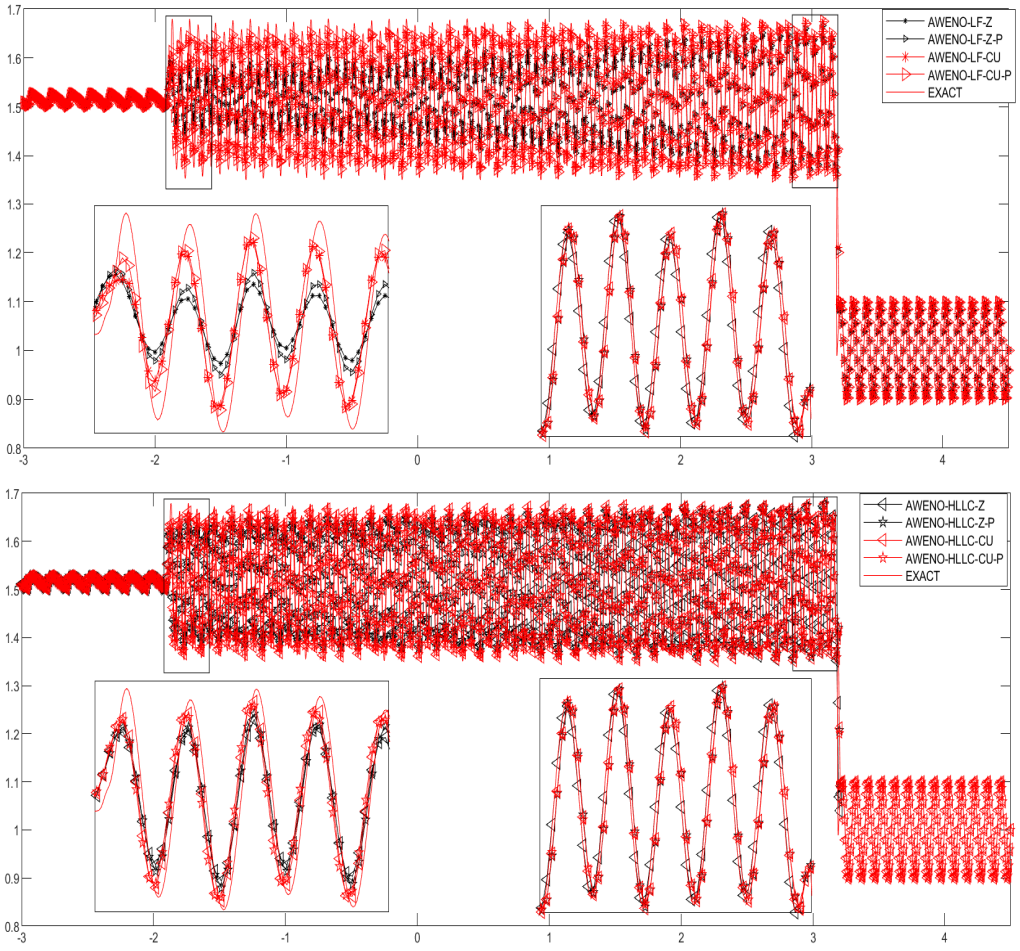

FIGURE 2. Density profiles of shock/turbulence interaction problem [43] with 1500 grid points at $t = 5$.

In addition, we consider the modified shock wave and turbulence interaction problem [43] with initial data:

$$(\rho, u, p) = \begin{cases} (1.515695, 0.523346, 1.80500) & \text{for } x \in [-5, -4), \\ (1 + 0.1\sin(20\pi x), 0, 1) & \text{for } x \in [-4, 5]. \end{cases}$$

The simulation was performed until time $t = 5$ for the grid with $\Delta x = 1/150$. The numerical results are displayed in Fig. 2. The sinusoidal wave pattern behind the shock-entropy wave interactions is better captured by AWENO-CU-P than other AWENO methods.

Example 4.3. (*Sod problem*) The 1D shock tube test by Sod [44] uses the initial condition given by

$$(\rho, u, p) = \begin{cases} (1, 0, 1) & \text{for } x \in [0, 0.5), \\ (0.125, 0, 0.1) & \text{for } x \in [0.5, 1], \end{cases}$$

with $\gamma = 1.4$. The exact solution is obtained from the exact Riemann solver reported by Toro [45]. We compute this problem with $\Delta x = 1/200$ until the final time $t = 0.2$. In Fig. 3, the density distributions ρ predicted by the six AWENO schemes are compared with the exact solution; all perturbational AWENO schemes have no oscillation near shock or contact wave. We can say that new tunable functions φ_5 and φ_6 successfully control the high order derivative terms while maintaining the non-oscillatory properties. The perturbational AWENO schemes produce better results when compared to their original schemes; the AWENO-CU-P produces best results for both flux functions.

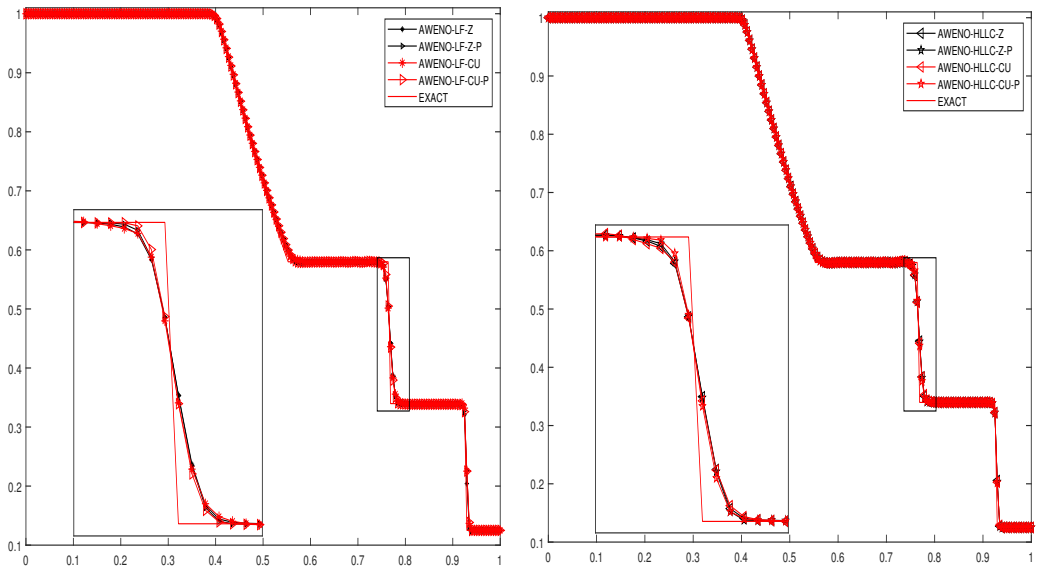

FIGURE 3. Density profiles of Sod problem [44] with 200 grid points at $t = 0.2$.

Example 4.4. (*Lax problem*) Now, we test 1D Euler equations for the Lax problem [46] which is the initial data given by

$$(\rho, u, p) = \begin{cases} (0.445, 0.698, 3.528) & \text{for } x \in [-5, 0), \\ (0.5, 0, 0.571) & \text{for } x \in [0, 5] \end{cases}$$

with $\gamma = 1.4$ and $\Delta x = 10/200$. In Fig. 4 we present the density profiles ρ of exact solution (reported in Toro [45]) and the density profiles ρ computed by the AWENO schemes. We

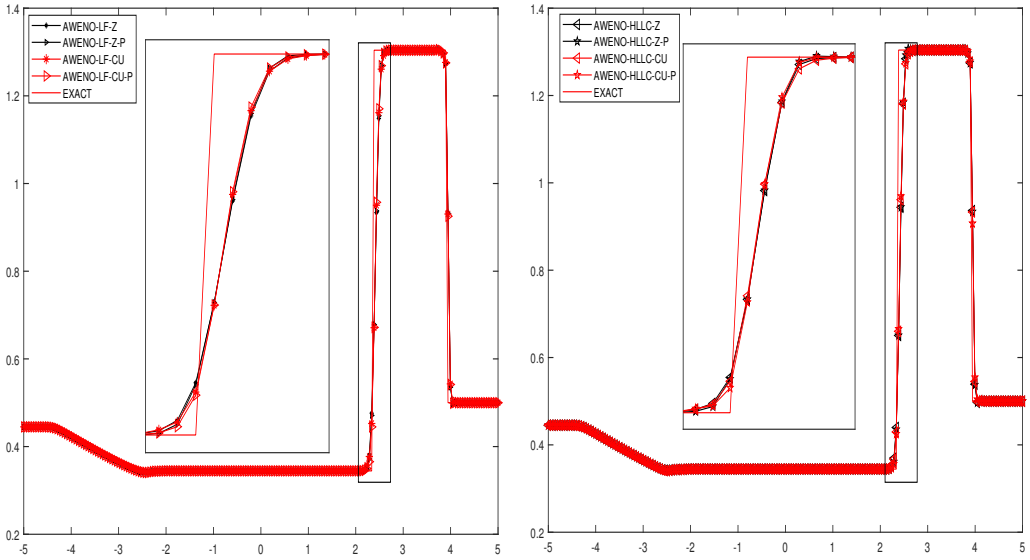

FIGURE 4. Density profiles of Lax problem [46] with 200 grid points at $t = 1.6$.

notice again that all AWENO schemes maintain non-oscillatory properties. We can see that the AWENO-CU-P scheme (with LF or HLLC) shows very stiff transition near contact and shock discontinuities.

Example 4.5. (*Blast wave problem*) The famous test problem proposed by Woodward and Colella [47] is considered to investigate the behavior of proposed schemes under interactions of two strong shock waves. The initial conditions of this problem are set by

$$(\rho, u, p) = \begin{cases} (1, 0, 1000) & \text{for } x \in [0, 0.1), \\ (1, 0, 0.01) & \text{for } x \in [0.1, 0.9], \\ (1, 0, 100) & \text{for } x \in [0.9, 1]. \end{cases}$$

The reflective wall boundary condition is applied to the both edges of the domain. The final computational time is $t = 0.038$ with $\Delta x = 1/400$. The reference solution is obtained from the fifth-order WENO-JS scheme [9] with 3200 grid points. The density profiles ρ yielded by AWENO schemes are presented in Fig. 5; all AWENO schemes maintain the non-oscillatory properties even in very strong shockwave interactions. Each original AWENO scheme is improved by perturbational terms. Also, the results of AWENO-Z-P and AWENO-CU-P are closer to the reference solutions than the others. The AWENO-CU-P scheme achieves the highest resolution in resolving the peak of the density profile for each flux function case.

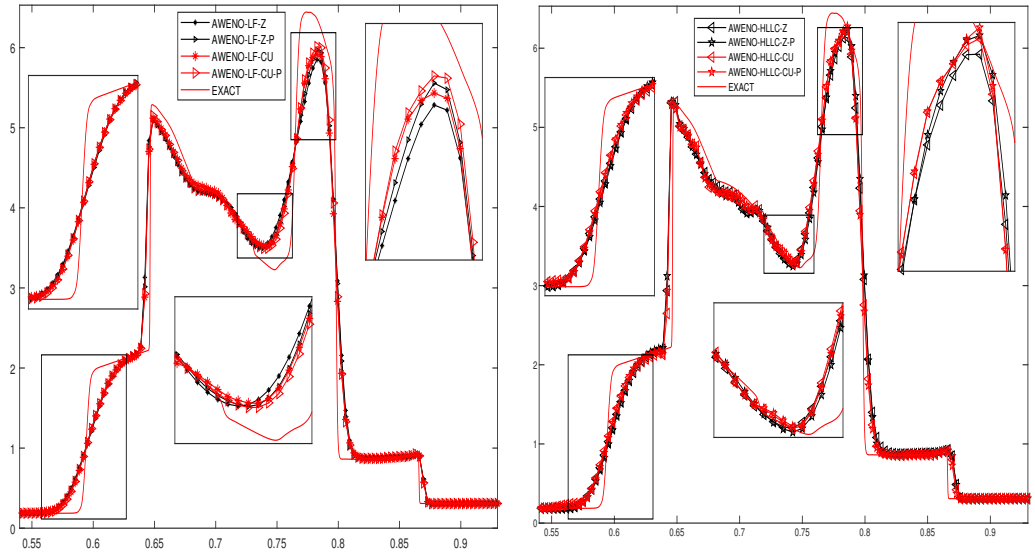

FIGURE 5. Density profiles of blast wave problem [47] with 400 grid points at $t = 0.038$.

4.3. **2D Euler Systems.** In this section, we present the numerical results to investigate behaviors of proposed AWENO schemes in 2D compressible Euler equations. We specify the specific heat ratio $\gamma = 1.4$ for all 2D problems except the Rayleigh-Taylor instability problem.

Example 4.6. (*Two-dimensional Riemann problem - configuration* 3) We consider well-known the third configuration of the 2D Riemann problems proposed in [48]. The square, $[0,1]\times[0,1]$, computational domain is partitioned into four section by vertical line $x = 0.8$ and horizontal line $y = 0.8$. The initial data on each quadrant is given as:

$$(\rho, u, v, p) = \begin{cases} (1.5, 0, 0, 1.5) & \text{for } (x,y) \in [0.8,1] \times [0.8,1], \\ (0.5323, 1.206, 0, 0.3) & \text{for } (x,y) \in [0,0.8] \times [0.8,1], \\ (0.138, 1.206, 1.206, 0.029) & \text{for } (x,y) \in [0,0.8] \times [0,0.8], \\ (0.5323, 0, 1.206, 0.3) & \text{for } (x,y) \in [0.8,1] \times [0,0.8] \end{cases}$$

and all boundaries are treated as outflow. We solve this problem until time $t = 0.8$ and compare the density contours of AWENO schemes in Fig. 6.

We can see that all schemes successfully produced solutions without non-physical oscillations near contact and shock discontinuities. Also, the AWENO-CU-P scheme captures the instability near the jet with high resolution. The vortex roll-ups on the slip line are sensitively affected by the numerical dissipation; the AWENO-HLLC-CU-P is the least dispersed among the proposed AWENO methods.

Example 4.7. (*Two-dimensional Riemann problem - configuration* 6) We now solve configuration 6 of the 2D Riemann problems [48]. The square, $[0,1] \times [0,1]$, computational domain is and partitioned by vertical line $x = 0.5$ and horizontal line $y = 0.5$. The initial data on each quadrant is given as:

$$(\rho, u, v, p) = \begin{cases} (1.0, 0.750, -0.50, 1.0) & \text{for } (x,y) \in [0.8,1] \times [0.5,1], \\ (2.0, 0.750, 0.50, 1.0) & \text{for } (x,y) \in [0,0.8] \times [0.5,1], \\ (1.0, -0.750, 0.50, 1.0) & \text{for } (x,y) \in [0,0.8] \times [0,0.5], \\ (3.0, -0.750, -0.50, 1.0) & \text{for } (x,y) \in [0.8,1] \times [0,0.5]. \end{cases}$$

We computed this problem until the final time $t = 1.0$ and displayed the density contour lines in Fig. 7. The perturbational schemes have more rich and fine structures around the center of vortex when they are compared with those original AWENO schemes; the AWENO-CU-P schemes generates many and large rollups along the interfaces.

Example 4.8. (*Two-dimensional Rayleigh-Taylor instability*) Many authors (e.g., [49, 50]) have simulated this problem to check the numerical dissipation of their high-order accurate schemes. The computational area, $[0, 0.25] \times [0, 1]$, is divided by 160 $\times$ 640 meshes. The initial value is given by

$$(\rho, u, v, p) = \begin{cases} (2, 0, -0.025\sqrt{\dfrac{5p}{3\rho}}\cos(8\pi x), 2y+1) & \text{for } y \in [0, 0.5), \\ (1, 0, -0.025\sqrt{\dfrac{5p}{3\rho}}\cos(8\pi x), y+1.5) & \text{for } y \in [0.5, 1]. \end{cases}$$

This problem simulates interfacial instability caused by two fluids with different densities. The heavier gas penetrates to the lighter gas and it is accelerated by gravitational force. The gravitational effect can be emulated by adding source term $(0, 0, \rho, \rho v)$ to the right side of Euler equation. Only for this problems, the specific heat ratio $\gamma = 5/3$ is considered. The right and left boundaries are treated as reflective wall; speed of x direction, u is reversed along the each boundary. Top and bottom boundaries are assigned as $(2, 0, 0, 1)$ and $(1, 0, 0, 2.5)$, respectively. The results at time $t = 1.95$ are displayed in Fig. 8. According to analysis in [49, 50], the details of complex structures originated in physical instability are affected by the numerical viscosity of specific scheme. The appearance of the fine structures near interface is an indicator of the inherent numerical viscosity. The HLLC cases have much more vortexes because the HLLC flux function is less dissipative. The perturbational schemes have more vortexes near the plume. The AWENO-CU-P scheme makes regular vortexes at the interface whereas the AWENO-CU scheme makes irregular vortexes. We can say that the perturbational terms greatly improve contact discontinuous resolution.

Example 4.9. (*Double Mach reflection of strong shock waves*) This problem is introduced by Woodward and Colella [47]. The Mach 10 high speed flow crashes into the oblique ramp with 60°; multiple shock wave reflection and Mach stem generates complex structures and slip lines. We model this problem in the computational domain $[0, 4] \times [0, 1]$. The oblique ramp

is aligned along the horizontal axis and the edge of ramp is posed at the point $(x, y) = (\frac{1}{6}, 0)$. The Mach 10 right-moving flow with density $\rho = 1.4$ and pressure $p = 1$ is imposed in front of edge and exact post-shock condition is applied behind the edge. The upper boundary is treated as moving shock wave with Mach 10. The left and right boundaries use inflow and outflow boundary conditions, respectively. The simulation was performed until the final time $t = 0.2$ with 1200×300 grid. The density contour around the Mach stem are presented in Fig. 9. We can clearly notice that the perturbational schemes have the better resolution near the Kelvin–Helmholtz vortex; the AWENO-CU-P shows good resolution even in corse mesh. Additionally, all perturbational schemes capture strong shockwave and Mach stem without non-physical oscillations.

Example 4.10. (*Explosion*) We compute the explosion problem proposed in [45] (see also [51]) which is a circularly symmetric problem with initial circular region of high density and pressure. We compute on the domain $[-1.5, 1.5] \times [-1.5, 1.5]$ and center of the high pressure region is posed on the origin. The initial conditions are

$$(\rho, u, v, p) = \begin{cases} (1.000, 0, 0, 1.0) & \text{if } x^2 + y^2 < 0.16, \\ (0.125, 0, 0, 0.1) & \text{otherwise.} \end{cases}$$

We compute the solution until the final time $t = 3.2$ with 800×800 mesh grids and display the density contour obtained from AWENO schemes in Fig. 10. The numerical result produced by AWENO-CU-P is much more "curlier" than that of other methods at the contact surface. The AWENO-CU-P has substantially reduced dissipation when compared to other AWENO schemes.

5. Conclusion

In this paper, we proposed improved fifth- and sixth-order AWENO methods which add perturbational terms to the conserved vectors for the numerical solution of the hyperbolic conservation laws. The proposed schemes maintain the fifth- and sixth-order accuracy in smooth regions even at critical points and produce high resolutions around singularities of the derivatives. Extensive numerical experiments have been presented to explain the effectiveness and less-dissipation of the new schemes. Also, proposed schemes resolve discontinuities sharply while maintaining an essentially non-oscillatory performance.

6. Appendix

- **The Lax-Friedrichs (LF) flux.** The LF flux is defined by

$$\hat{f}^{\mathrm{LF}}_{j+1/2}(q^-, q^+) = \frac{1}{2}[(f(q^-) + f(q^+)) - \alpha(q^+ - q^-)],$$

where α is taken as an upper bound over the whole line for $|f'(q)|$ in the scalar case, or the absolute value of eigenvalues of the Jacobian for the system case.

• **The HLLC flux.** The HLLC flux is a modified version of the HLL flux, whereby the missing contact and shear waves are restored. The HLLC flux for the Euler equations $q = (\rho, \rho u, E)^T$ is given by

$$\hat{f}^{\mathrm{HLLC}}_{j+1/2}(q^-, q^+) = \begin{cases} f(q^-) & \text{if } 0 \le s^-, \\ f(q^-) + s^-(q^{0-} - q^-) & \text{if } s^- \le s^0, \\ f(q^+) + s^+(q^{0+} - q^+) & \text{if } s^0 \le s^+, \\ f(q^+) & \text{if } s^+ \le 0, \end{cases}$$

where, by defining the averaging operation $\bar{f} = \frac{1}{2}(f^+ + f^-)$ and the difference operation $\Delta f = f^+ - f^-$,

$$q^{0\pm} = \rho^{0\pm}\frac{s^\pm - u^\pm}{s^\pm - s^0}\begin{bmatrix} 1 \\ s^0 \\ \frac{E^\pm}{\rho^\pm} + (s^0 - u^\pm)\Big(s^0 + \frac{p^\pm}{s^\pm - u^\pm}\Big) \end{bmatrix},$$

$$p^0 = \bar{p} - \frac{1}{2}\Delta\bar{\rho}\bar{c}, \quad s^0 = \bar{u} - \frac{1}{2}\frac{\Delta p}{\bar{\rho}\bar{c}}, \quad s^\pm = u^\pm \pm c^\pm Q^\pm,$$

$$Q^\pm = \begin{cases} 1 & \text{if } p^0 \le p^\pm, \\ \Big(1 + \frac{\gamma+1}{2\gamma}\big(\frac{p^0}{p^\pm} - 1\big)\Big)^{1/2} & \text{if } p^\pm \le p^0. \end{cases}$$

Acknowledgements

This work was supported by the Challengeable Future Defense Technology Research and Development Program through the Agency for Defense Development(ADD) funded by the Defense Acquisition Program Administration in 2021(No. 915020201). Also, this work was supported by the grant of NRF-2021R1A2C1095443 and ICT R&D program of MOTIE (P0014715).

REFERENCES

[1] A. Harten, *High resolution schemes for hyperbolic conservation laws*, Journal of Computational Physics, **49** (1983), 357–393.

[2] A. Harten, *On a Class of High Resolution Total-Variation-Stable Finite-Difference Schemes*, SIAM Journal on Numerical Analysis, **21** (1984), 1–23.

[3] A. Harten, S. Osher, *Uniformly High-order Accurate Non-oscillatory Schemes*, IMRC Technical Summary Rept. 2823, University of Wisconsin, Madison, WI, 1985.

[4] A. Harten and S. Osher, *Uniformly High-Order accurate Non-Oscillatory schemes. I*, SIAM Journal on Numerical Analysis, **24** (1987), 279–309.

[5] A. Harten, B. Engquist, S. Osher, and S. Chakravarthy, *Uniformly High-Order accurate Non-Oscillatory schemes, III*, Journal of Computational Physics, **71** (1987), 231–303.

[6] C.W. Shu and S. Osher, *Efficient implementation of essentially non-oscillatory shock capturing schemes*, Journal of Computational Physics, **77** (1988), 439–471.

[7] C.W. Shu and S. Osher, *Efficient implementation of essentially non-oscillatory shock capturing schemes, II*, Journal of Computational Physics, **83** (1989), 32–78.

[8] X.-D. Liu, S. Osher, and T. Chan, *Weighted essentially non-oscillatory schemes*, Journal of Computational Physics, **115** (1994), 200–212.

[9] G. Jiang and C.W. Shu, *Efficient implementation of weighted ENO schemes*, Journal of Computational Physics, **126** (1996), 202–228.
[10] A.K. Henrick, T.D. Aslam, and J.M. Powers, *Mapped weighted-essentially-non-oscillatory schemes : achieving optimal order near critical points*, Journal of Computational Physics, **207** (2005), 542–567.
[11] R. Borges, M. Carmona, B. Costa, and W.S. Don, *An improved WENO scheme for hyperbolic conservation laws*, Journal of Computational Physics, **227** (2008), 3191–3211.
[12] F. Acker, R. B. de R. Borges and B. Costa, *An improved WENO-Z scheme*, Journal of Computational Physics, **313** (2016), 726-753.
[13] S. Gottlieb, J. S. Mullen, and S.J. Ruuth, *A Fifth Order Flux Implicit WENO Method*, Journal of Scientific Computing, **27** (2006), 271-287.
[14] Y. Ha, C. H. Kim, Y. J. Lee, and J. Yoon, *An improved weighted essentially non-oscillatory scheme with a new smoothness indicator*, Journal of Computational Physics, **232** (2013), 68–86.
[15] C. H. Kim, Y. Ha, and J. Yoon, *Modified non-linear weights for fifth-order weighted essentially non-oscillatory schemes*, Journal of Scientific Computing, **67** (2016), 299-323.
[16] J. Zhu, J.X. Qiu, *A new fifth order finite difference WENO scheme for solving hyperbolic conservation laws*, Journal of Computational Physics, **318** (2016), 110–121.
[17] X. Y. Hu Q. Wang, and N. A. Adams, *An adapive central-upwind weighted essentially non-oscillatory scheme*, Journal of Computational Physics, **229** (2010), 8952–8965.
[18] X. Y. Hu, and N. A. Adams, *Scale separation for implicit large eddy simulation*, Journal of Computational Physics, **230** (2011), 7240–7249.
[19] D.S. Balsara and C.W. Shu, *Monotonicity preserving WENO schemes with increasingly high-order of accuracy*, Journal of Computational Physics, **160** (2000), 405–452.
[20] G.A. Gerolymos, D.Sénéchal, and I. Vallet, *Very-high-order WENO schemes*, Journal of Computational Physics, **228** (2009), 8481–8524.
[21] Y. Ha, C. H. Kim, Y. H. Yang, and J. Yoon, *Sixth-order weighted essentially non-oscillatory schemes based on exponential polynomials*, SIAM Journal on Scientific Computing, **38** (2016), A1987–A2017.
[22] I. Cravero, M. Semplice, *On the accuracy of WENO and CWENO reconstructions of third order on nonuniform meshes*, Journal of Scientific Computing, **67** (2016), 1219–1246.
[23] M. Käser, A. Iske, *ADER schemes on adaptive triangular meshes for scalar conservation laws*, Journal of Computational Physics, **205** (2005), 486–508.
[24] D. Levy, G. Puppo, G. Russo, *Central WENO schemes for hyperbolic systems of conservation laws*, Mathematical Modelling and Numerical Analysis, **33** (1999), 547–571.
[25] S. Pirozzoli, *Conservative hybrid compact-WENO schemes for shock–turbulence interaction*, Journal of Computational Physics, **178** (2002), 81–117.
[26] Y. Q. Shen, G.W. Yang, *Hybrid finite compact-WENO schemes for shock calculation*, International Journal for Numerical Methods in Fluids, **53** (2007), 531–560.
[27] D.S. Balsara, S. Garain, C.-W. Shu, *An efficient class of WENO schemes with adaptive order*, Journal of Computational Physics, **326** (2016), 780–804.
[28] L. L. Chen, C. Huang, *An improved WLS-WENO method for solving hyperbolic conservation laws*, Journal of Computational Physics, **392** (2019), 96–114.
[29] D. Levy, G. Puppo, G. Russo, *Compact central WENO schemes for multidimensional conservation laws*, SIAM Journal on Scientific Computing, **22** (2000), 656–672.
[30] H.X. Liu, X.M. Jiao, *WLS-ENO: weighted-least-squares based essentially non-oscillatory schemes for finite volume methods on unstructured meshes*, Journal of Computational Physics, **314** (2016), 749–773.
[31] R. Zhang, M. Zhang, C.-W. Shu, *On the order of accuracy and numerical performance of two classes of finite volume WENO schemes*, Communications in Computational Physics, **5** (2009), 836–848.
[32] J. Zhu, J.X. Qiu, *A new type of finite volume WENO schemes for hyperbolic conservation laws*, Journal of Scientific Computing, **73** (2017), 1338–1359.

[33] F. Zeng, Y. Shen, S. Liu, *A perturbational weighted essentially non-oscillatory scheme*. Computer and Fluids, **172** (2018), 196–208.
[34] Yahui Wang, Yulong Du, Kunlei Zhao and Li Yuan, *Modified Stencil Approximations for Fifth-Order Weighted Essentially Non-oscillatory Schemes*, Journal of Scientific Computing, **81** (2019), 898–922.
[35] Y. Jiang, C.W. Shu, M.P. Zhang, *An alternative formulation of finite difference weighted ENO schemes with Lax-Wendroff time discretization for conservation laws*, SIAM Journal on Scientific Computing, **35** (2013), 137–160.
[36] Y. Jiang, C.W. Shu, M.P. Zhang, *Free-stream preserving finite difference schemes on curvilinear meshes*, Methods and Applications of Analysis, **21** (2014), 1–30.
[37] H. Liu, *A numerical study of the performance of alternative weighted ENO methods based on various numerical fluxes for conservation law*, Applied Mathematics and Computation, **296** (2017), 182–197.
[38] Bao-Shan Wang, Peng Li, Zhen Gao, Wai Sun Don, *An improved fifth order alternative WENO-Z finite difference scheme for hyperbolic conservation laws*, Journal of Computational Physics, **374** (2018), 469–477.
[39] M. Castro, B. Costa, and W.S. Don, *High Order Weighted Essentially Non-Oscillatory WENO-Z schemes for hyperbolic conservation laws*, Journal of Computational Physics, **230** (2011), 1766–1792 (2011).
[40] H. Liu, J. Qiu, *Finite difference Hermite WENO schemes for conservation laws, II: An alternative approach*, Journal of Scientific Computing, **66** (2016), 598–624.
[41] Bao-Shan Wang, Wai Sun Don, Naveen K. Garg, Alexander Kurganov, *Fifth-order A-weno finite-difference schemes based on a new adaptive diffusion central numerical flux*, SIAM Journal on Scientific Computing, **42** (2020), A3932–A3956.
[42] C.W. Shu, *ENO and WENO schemes for hyperbolic conservation laws, in: B. Cockburn, C. Johnson, C.W. Shu, E. Tadmor (Eds.)*, Advanced Numerical Approximation of Nonlinear Hyperbolic Equations, Lecture Notes in Mathematics, vol. 1697, Springer, Berlin, 1998, 325–432 (also NASA CR- 97-206253 and ICASE-97-65 Rep., NASA Langley Research Center, Hampton [VA, USA]).
[43] V. A. Titarev, E. F. Toro, *Finite-volume WENO schemes for three-dimensional conservation laws*, Journal of Computational Physics, **201** (2004), 238–260.
[44] G. Sod, *A Survey of Several Finite Difference Methods for Systems of Nonlinear Hyperbolic Conservation Laws*, Journal of Computational Physics, **27** (1978), 1–31.
[45] E.F. Toro, *Riemann Solvers and Numerical Methods for Fluid Dynamics*, Springer-Verlag, New York, 1997.
[46] P.D. Lax, *Weak solutions of Nonlinear Hyperbolic Equations and their Numerical Computation*, Communications on Pure and Applied Mathematics, **7** (1954), 159 –193.
[47] P. Woodward and P. Colella, *The Numerical Simulation of Two-Dimensional Fluid Flow with Strong Shocks*, Journal of Computational Physics, **54** (1984), 115–173.
[48] C.W. Schulz-Rinne, J.P. Collins, and H.M. Glaz, *Numerical Solution of the Riemann Problem for Two-Dimensional Gas Dynamics*, SIAM Journal on Scientific Computing, **14** (1993), 1394–1414.
[49] Y. Shi, Y. Guo, *A fifth order alternative Compact-WENO finite difference scheme for compressible Euler equations*, Journal of Computational Physics, **397** (2019), 108873.
[50] Z.F. Xu, C.W. Shu, *Anti-diffusive flux corrections for high order finite difference WENO schemes*, Journal of Computational Physics, **205** (2005), 458–485.
[51] R. Liska and B. Wendroff, *Comparison of several difference schemes on 1D and 2D test problems for the Euler equations*, SIAM Journal on Scientific Computing, **25** (2004), 995–1017.

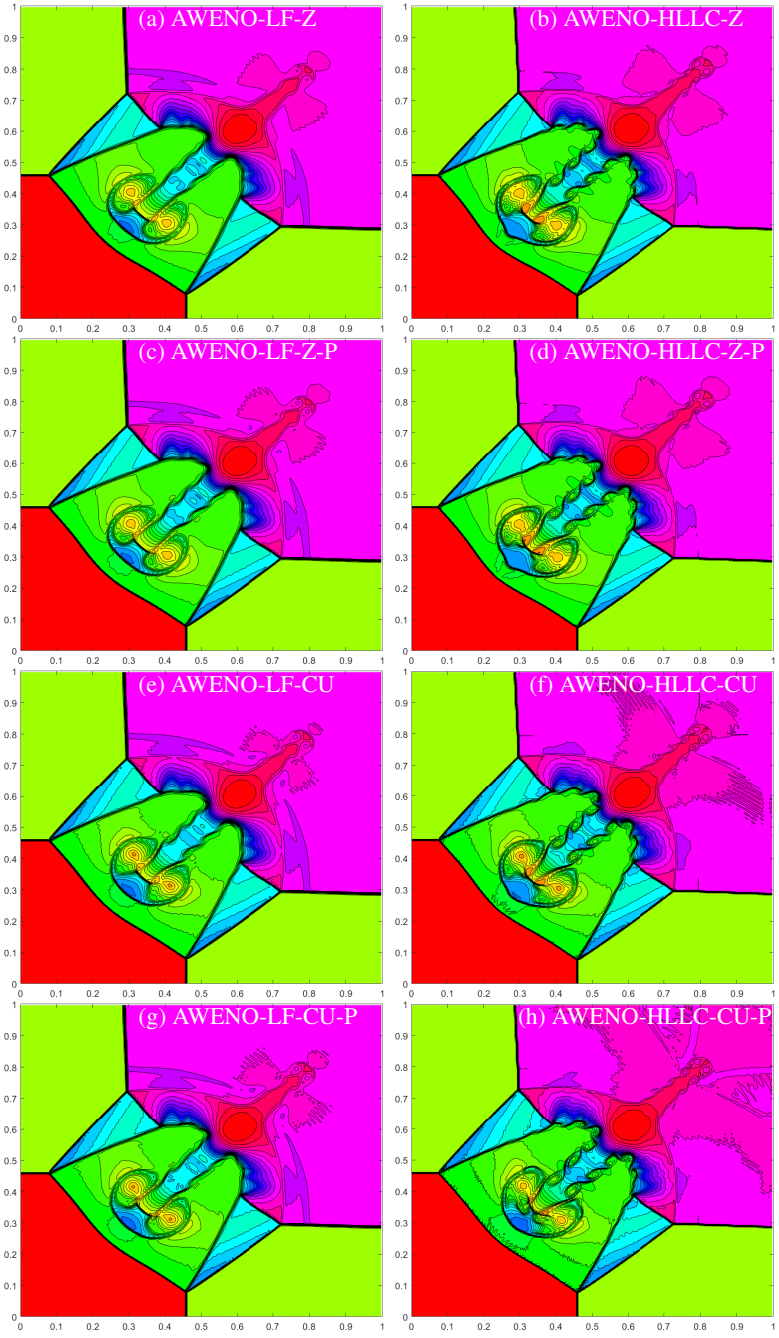

FIGURE 6. 2D Riemann problem-configuration 3 at $t = 0.8$ (density profiles, 300×300).

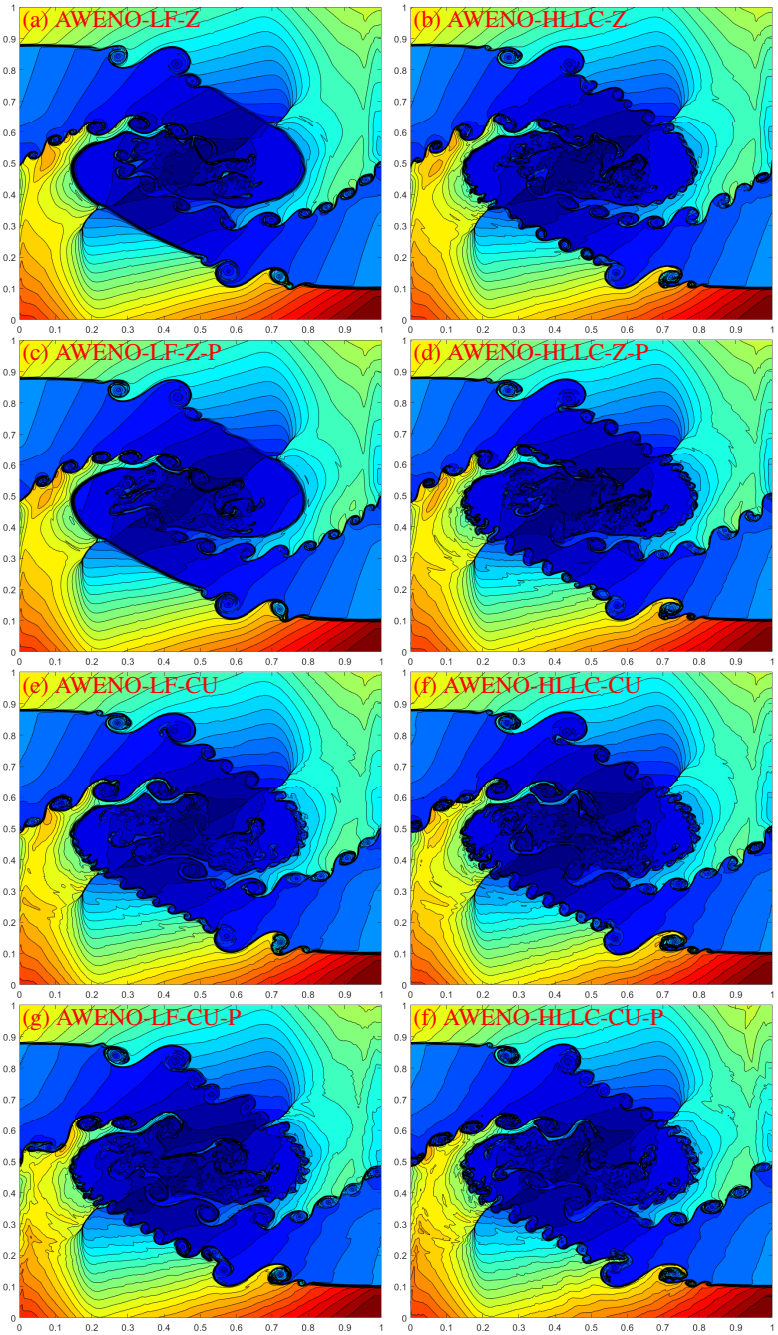

FIGURE 7. 2D Riemann problem-configuration 6 at $t = 1.0$ (density profiles, 800×800).

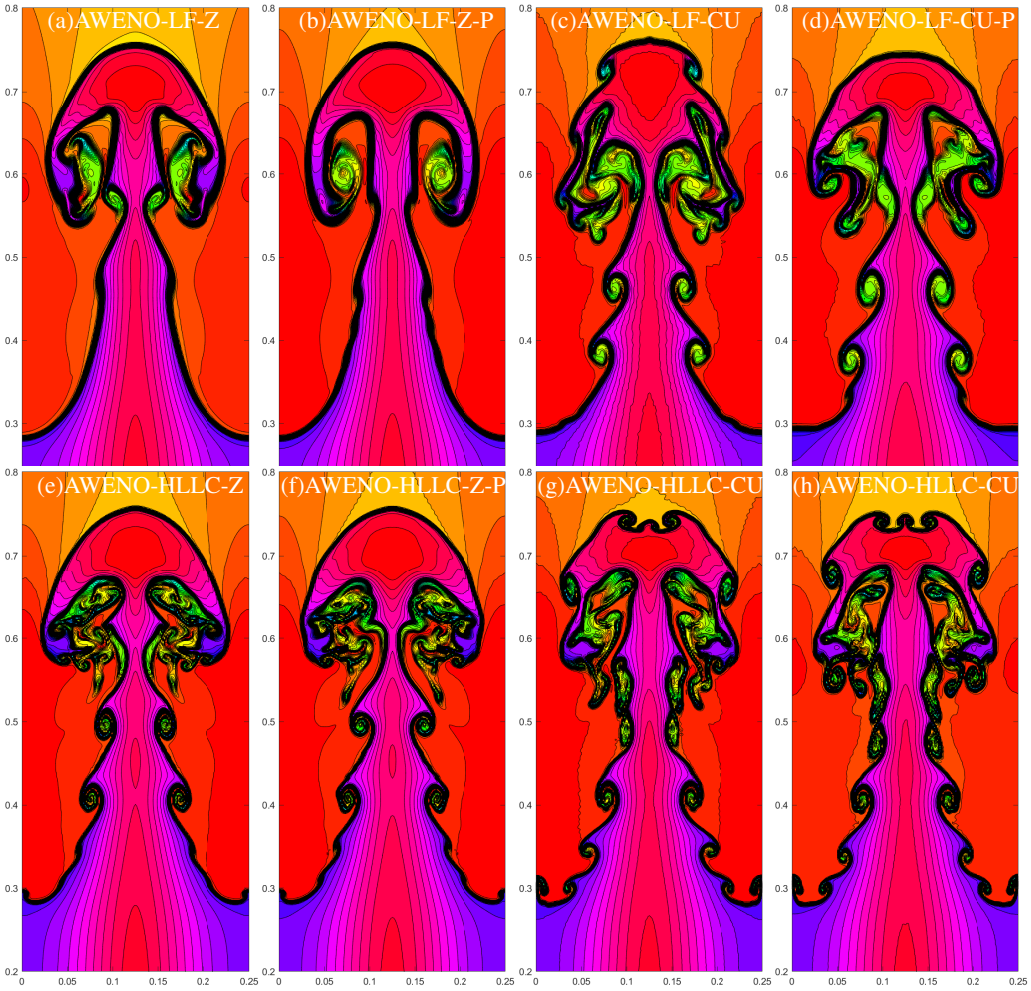

FIGURE 8. Rayleigh-Taylor instability at $t = 1.95$ (density profiles, 160×640).

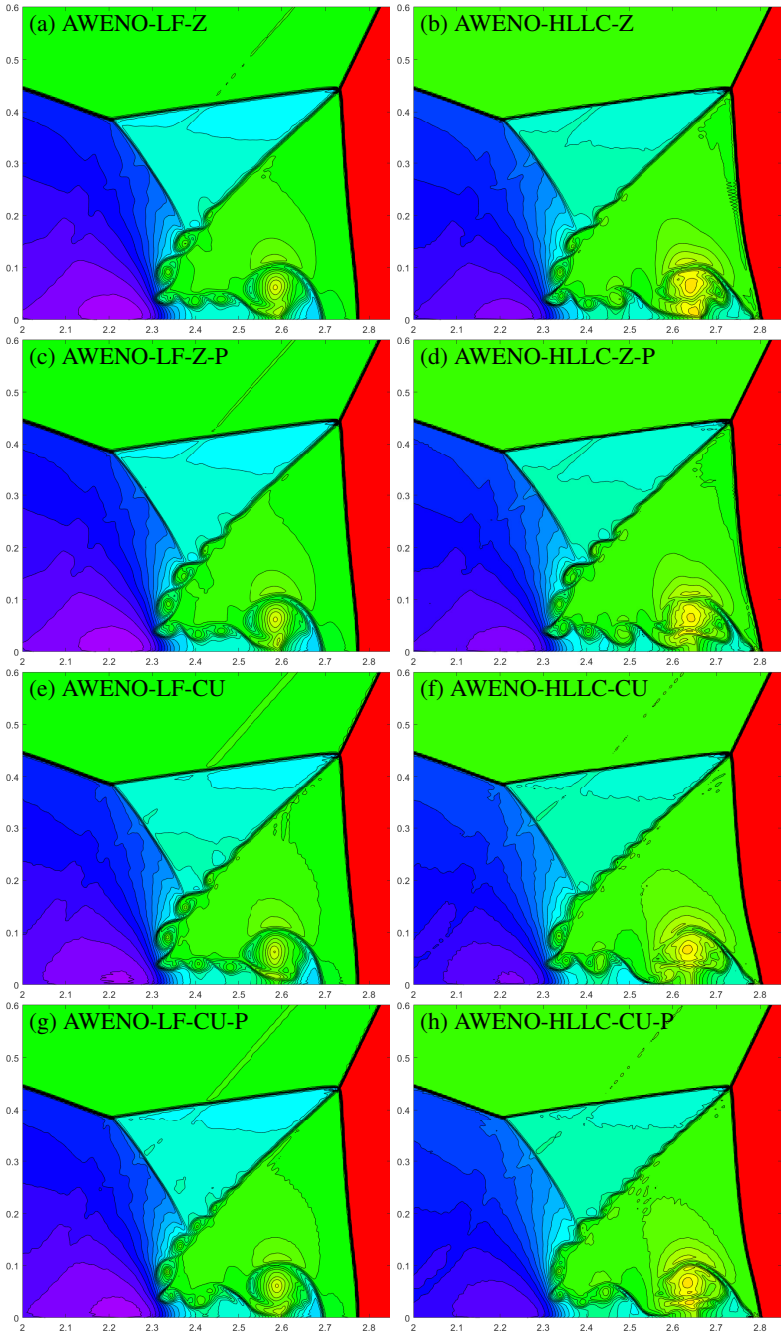

FIGURE 9. Double Mach reflection of a strong shock [47] at $t = 0.2$ (density profiles, 1200×300).

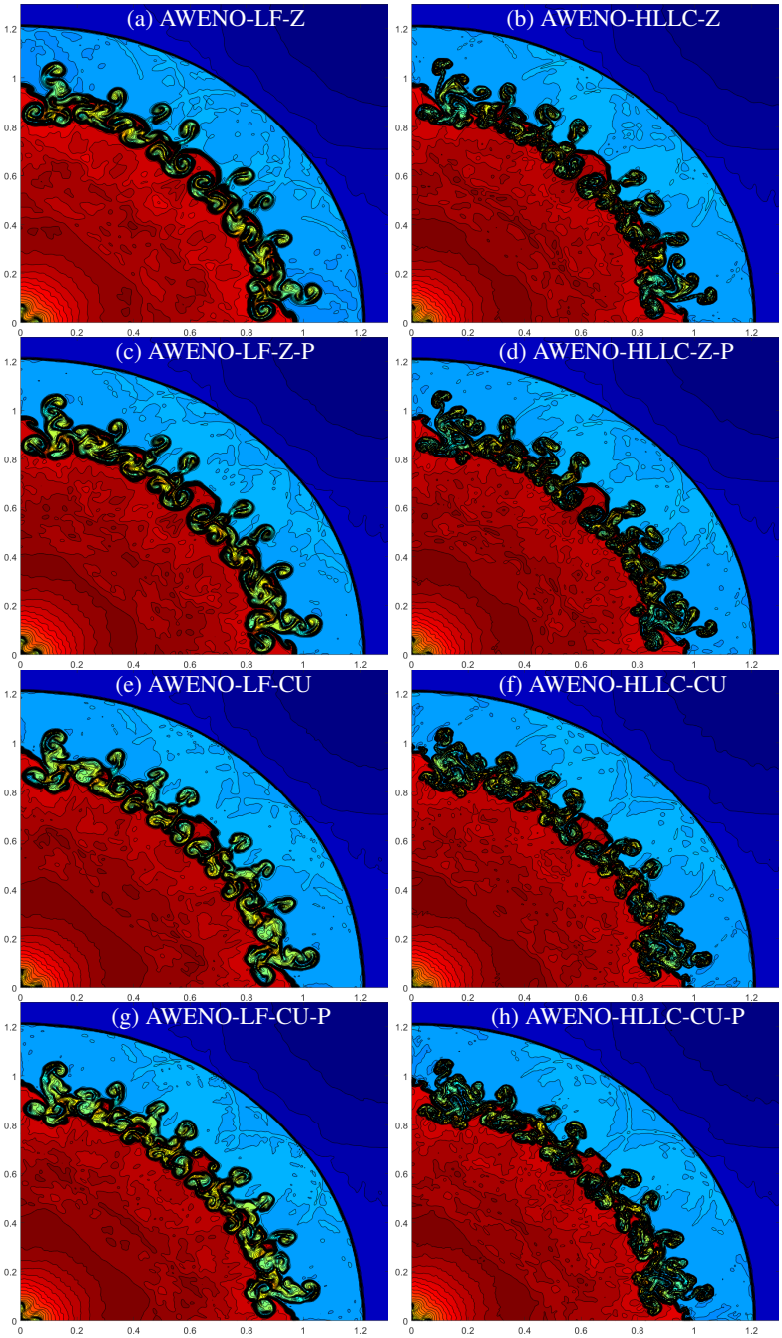

FIGURE 10. Explosion problem [45] at $t = 3.2$ (density profiles of first quadrant, 800×800).